AGU PUBLICATIONS

JGR

Journal of Geophysical Research: Space Physics

RESEARCH ARTICLE
10.1002/2014JA020878

Key Points:
- Majority of postmidnight EPBs during June solstice are freshly evolving type
- Equatorward meridional wind plays a major role in postmidnight-evolving EPBs
- Large number of EPBs evolved a few minutes prior to apex sunset during equinox

Correspondence to:
S. T. Ram,
tulasi@iigs.iigm.res.in

Citation:
Ajith, K. K., S. T. Ram, M. Yamamoto, T. Yokoyama, V. S. Gowtam, Y. Otsuka, T. Tsugawa, and K. Niranjan (2015), Explicit characteristics of evolutionary-type plasma bubbles observed from Equatorial Atmosphere Radar during the low to moderate solar activity years 2010–2012, *J. Geophys. Res. Space Physics*, *120*, doi:10.1002/2014JA020878.

Received 25 NOV 2014
Accepted 7 JAN 2015
Accepted article online 11 JAN 2015

Explicit characteristics of evolutionary-type plasma bubbles observed from Equatorial Atmosphere Radar during the low to moderate solar activity years 2010–2012

K. K. Ajith[1], S. Tulasi Ram[1], M. Yamamoto[2], T. Yokoyama[3], V. Sai Gowtam[1], Y. Otsuka[4], T. Tsugawa[3], and K. Niranjan[5]

[1]Indian Institute of Geomagnetism, Navi Mumbai, India, [2]Research Institute for Sustainable Humanosphere, Kyoto University, Uji, Japan, [3]National Institute of Information and Communications Technology, Tokyo, Japan, [4]Solar Terrestrial Environment Laboratory, Nagoya University, Nagoya, Japan, [5]Department of Physics, Andhra University, Visakhapatnam, India

Abstract Using the fan sector backscatter maps of 47 MHz Equatorial Atmosphere Radar (EAR) at Kototabang (0.2°S geographic latitude, 100.3°E geographic longitude, and 10.4°S geomagnetic latitude), Indonesia, the spatial and temporal evolution of equatorial plasma bubbles (EPBs) were examined to classify the evolutionary-type EPBs from those which formed elsewhere and drifted into the field of view of radar. A total of 535 EPBs were observed during the low to moderate solar activity years 2010–2012, out of which about 210 (~39%) are of evolving type and the remaining 325 (~61%) are drifting-in EPBs. In general, both the evolving-type and drifting-in EPBs exhibit predominance during the postsunset hours of equinoxes and December solstices. Interestingly, a large number of EPBs were found to develop even a few minutes prior to the apex sunset during equinoxes. Further, the occurrence of evolving-type EPBs exhibits a clear secondary peak around midnight (2300–0100 LT), primarily, due to higher rate of occurrence during the postmidnight hours of June solstices. A significant number (~33%) of postmidnight EPBs generated during June solstices did not exhibited any clear zonal drift, while about 14% of EPBs drifted westward. Also, the westward drifting EPBs are confined only to June solstices. The responsible mechanisms for the genesis of fresh EPBs during postmidnight hours were discussed in light of equatorward meridional winds in the presence of weak westward electric fields.

1. Introduction

The equatorial plasma bubbles (EPBs)/equatorial spread *F* (ESF) irregularities are an important topic of space weather interest because of their impact on transionospheric radio communications, satellite-based navigation and augmentation systems. This local plasma-depleted structures develop at the bottom side *F* layer through Rayleigh-Taylor instability and rapidly grow to topside ionosphere via polarization electric fields within them. A series of cascading instability processes lead to the formation of wide spectrum of irregularities with scale sizes ranging from 10^{-2} to 10^{5} m [*Haerendel*, 1973; *Kelley*, 1989] that can affect a wide band of radio wave spectrum. A variety of instruments such as ionosondes, airglow photometers, coherent and incoherent backscatter radars, transionospheric scintillations, and satellite in situ probes are employed for probing the EPB/ESF irregularities at different scale sizes toward understanding the genesis, dynamics, and morphological characteristics of EPBs.

The EPBs are essentially a nighttime phenomena when the *E* region conductivity becomes negligible that liberates the polarization electric fields in *F* region to grow nonlinearly. The steep vertical gradients due to quick loss of bottomside ionization and rapid uplift of equatorial *F* layer via prereversal enhancement (PRE) of zonal electric field makes the postsunset hours as the most preferred local time for the formation of EPBs [*Kelley*, 1989; *Fejer et al.*, 1999; *Tulasi Ram et al.*, 2006]. Once developed, these EPBs generally drift eastward with velocities ranging from 50 to 200 m/s [*Aarons et al.*, 1980; *Bhattacharyya et al.*, 2001; *Rama Rao et al.*, 2005]. The seasonal and longitudinal variability of EPBs are influenced by the alignment between sunset terminator and magnetic meridian. The close alignment of sunset terminator with magnetic meridian causes simultaneous decay of *E* region conductivity at both ends of field line and maximizes the PRE [*Eccles*, 1998].

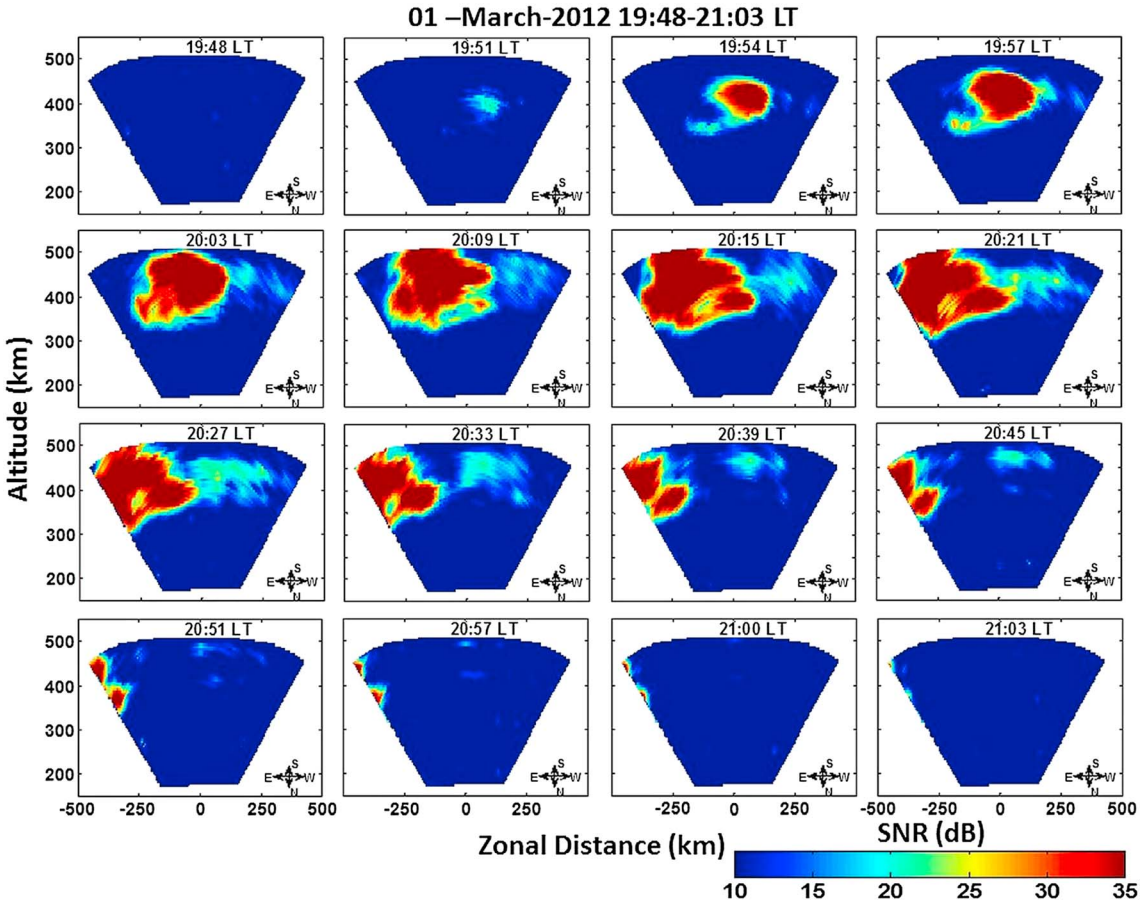

Figure 1. An example showing the genesis and successive development of EPB (evolving-type) over Kototabang observed from the fan sector maps of EAR on 1 March 2012.

In the Asian sector where the declination angle of geomagnetic field lines is nearly zero, EPB occurrence maximizes during the equinoxes and becomes less in solstices [*Tsunoda*, 1985; *Mendillo et al*., 1992; *Lee et al*., 2005; *Tulasi Ram et al*., 2006].

However, there is another class of irregularities that frequently occur during the postmidnight hours of June solstices over Asian sector which were earlier termed as class-II type by *Krishna Moorthy et al*. [1979]. This postmidnight irregularities maximizes during the low solar activity periods and are mostly associated with frequency-type spread *F* on ionograms [*Krishna Moorthy et al*., 1979; *Subbarao and Krishna Murthy*, 1994; *Sastri*, 1999; *Rama Rao et al*., 2005]. Using VHF backscatter radar at Kototabang in Indonesia, *Otsuka et al*. [2009] have reported that these postmidnight field-aligned irregularities (FAI) are generally weaker than those of premidnight EPBs and were not accompanied by GPS scintillations. Further, these summertime postmidnight irregularities often exhibit westward propagation though the majority of them do not show clear propagation. During the very low solar activity periods, the frequency of postmidnight irregularities of summer solstices may be even larger than the premidnight EPBs of equinoxes [*Heelis et al*., 2010; *Nishioka et al*., 2012]. *Yokoyama et al*. [2011b] have studied a few cases of postmidnight FAIs using Equatorial Atmosphere Radar (EAR) over Kototabang and simultaneous topside in situ observations from vector electric field instrument (VEFI) on board the C/NOFS (Communication/Navigation Outage Forecasting System) satellite. They have reported that these postmidnight FAIs can be active upwelling-type EPBs associated with rapid electric field fluctuations and need not be always fossil bubbles that are drifting into the field of view of radar. Later, *Nishioka et al*. [2012] have reported that uplift of *F* layer would play an important role in the evolution of fresh postmidnight FAIs over Kototabang. However, the reports of *Yokoyama et al*. [2011b] and *Nishioka et al*. [2012] were only case studies, and there is no statistical study on the frequency/probability of freshly evolving EPBs during postmidnight hours. Therefore, in the present statistical investigation, we distinguish the freshly

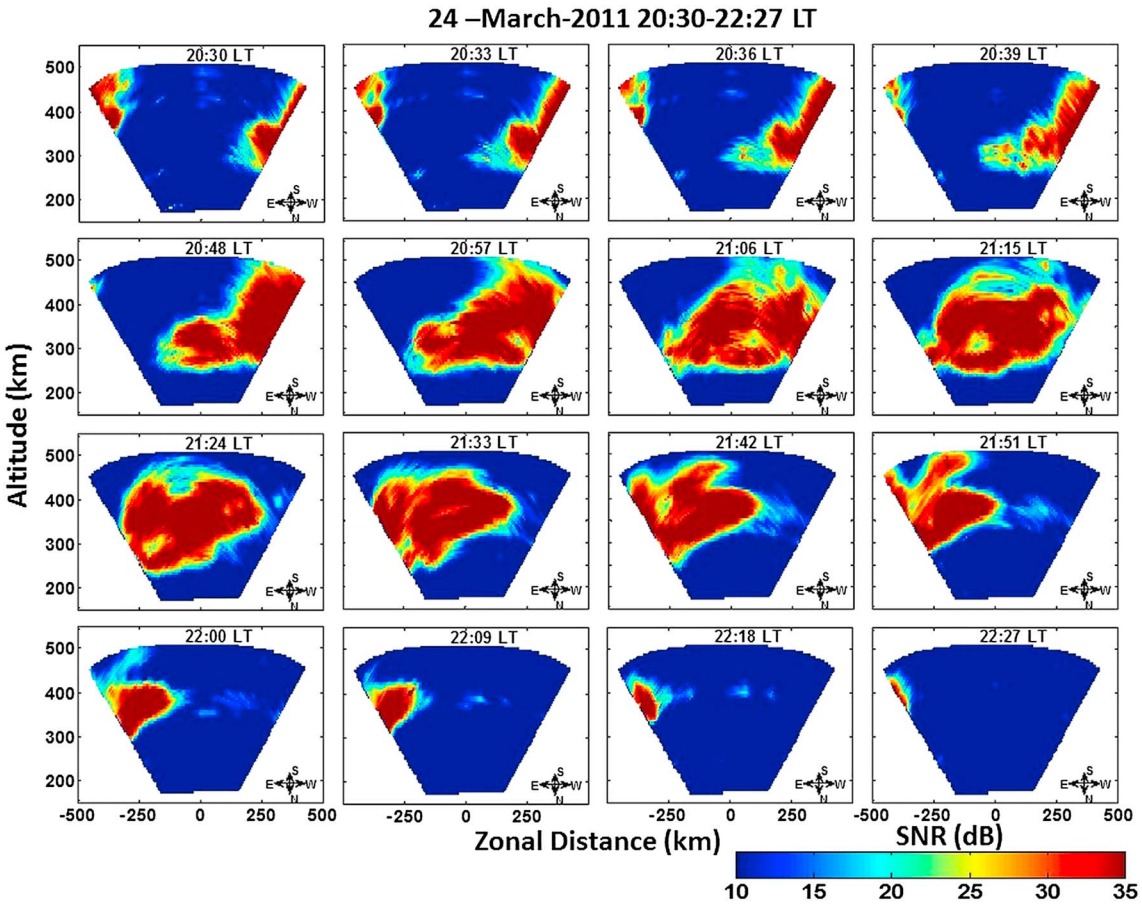

Figure 2. An example showing the drifting-in EPB entering from the western edge of fan sector map and drifting toward east on 24 March 2011.

evolved EPBs from those formed elsewhere and subsequently drifted into the field of view of radar, to explicitly study their local time, seasonal preferences, and zonal drift patterns over Kototabang.

Because of increasing reliability on satellite-based communication and navigation systems, the need of the hour is the prediction/forecasting of ionospheric scintillation in advance. There were also some recent attempts toward the deterministic prediction of scintillation based on the background ionospheric conditions at the afternoon hours [*Sridharan et al.*, 1994; *Thampi et al.*, 2006; *Sridharan et al.*, 2012]. However, not much progress has been made in those lines because the background conditions at the afternoon hours in those reports can only provide precursors for the development of postsunset EPBs over that location. On the other hand, the scintillation at any given location is not only determined by the EPBs developed over that location but also occurs due to the EPBs which are drifted in to that location. In addition, the evolutionary-type EPBs during the postmidnight hours of June solstices [*Yokoyama et al.*, 2011a; *Nishioka et al.*, 2012] adds further complexity for the prediction of ionospheric scintillation. Therefore, distinguishing the freshly evolving-type and drifting-in EPBs; and their distinct local time, seasonal preferences, and zonal drift characteristics provide important insights to improve the forecasting capability of ionospheric scintillations.

2. Observations

The Equatorial Atmosphere Radar (EAR) at Kototabang (0.2°S geographic latitude, 100.3°E geographic longitude, and 10.4°S geomagnetic latitude) operates at 47 MHz with a peak power of 100 kW and a beam width of 3.4° [*Fukao et al.*, 2003]. During nighttimes (18–06 LT), the EAR is generally operated in *F* region FAI mode to study the ESF irregularities at 3 m scales. Using the active-phased array antenna system, it can steer the beam on a pulse-to-pulse basis. The rapid beam-scanning ability enables the EAR to detect the temporal and spatial variations of backscatter plumes. In the present study, the nighttime equatorial plasma

Table 1. The Annual and Seasonal Occurrence Statistics of Both Evolving-Type and Drifting-In EPBs

	Equinox			June Solstice			December Solstice		
		No. of EPBs			No. of EPBs			No. of EPBs	
Year	Days Having Observation	Evolving Type	Drifting In	Days Having Observation	Evolving Type	Drifting In	Days Having Observation	Evolving Type	Drifting In
2010	68	16	34	66	12	12	48	0	1
2011	120	52	111	120	24	21	112	10	18
2012	120	64	98	121	21	25	113	11	5
Total	308	132	243	307	57	58	273	21	24

bubbles (EPBs) over Kototabang were studied using multibeam (16 beams) observations of EAR during the ascending phase of the solar cycle 24 (2010–2012 years). The annual mean $F_{10.7}$ solar flux for the years 2010–2012 are 80, 116, and 120 solar flux units, respectively, which indicates the low to moderate level of solar activity. The azimuth angles and ranges of these 16 beams were converted into zonal distance and vertical altitudes. The fan sector maps are constructed by combining the signal-to-noise ratio of back scatter echoes from the 16 beams. These fan sector backscatter maps has a wide east-west field of view (FoV) of ~500 km at 250 km altitude and ~800 km at 400 km altitude. This wide FoV of backscatter maps enabled us to observe the spatial and temporal evolution of EPBs over Kototabang. The data from two FMCW (frequency-modulated continuous wave) ionosondes operated at Chumphon (10.7°N geographic latitude, 99.4°E geographic longitude, and 3.3°N geomagnectic latitude) and Kototabang under SEALION (SouthEast Asia Low-latitude ionospheric network) have been used to study the background ionospheric conditions favorable for the development of EPBs.

In this study, the EPBs observed from EAR during the geomagnetically quiet ($Kp < 3$) periods of 2010–2012 are broadly classified into (i) evolving-type EPBs and (ii) drifting-in EPBs based on their spatial and temporal evolution. An EPB is considered as an evolving-type when it is originated within the FoV of EAR and found to grow successively. On the other hand, the developed EPBs entering from the western edge of FoV and drifting toward east were considered as drifting-in type EPBs. On some occasions, there were also some EPBs entering from the eastern edge of the FoV and drifting toward west during geomagnetically quiet periods.

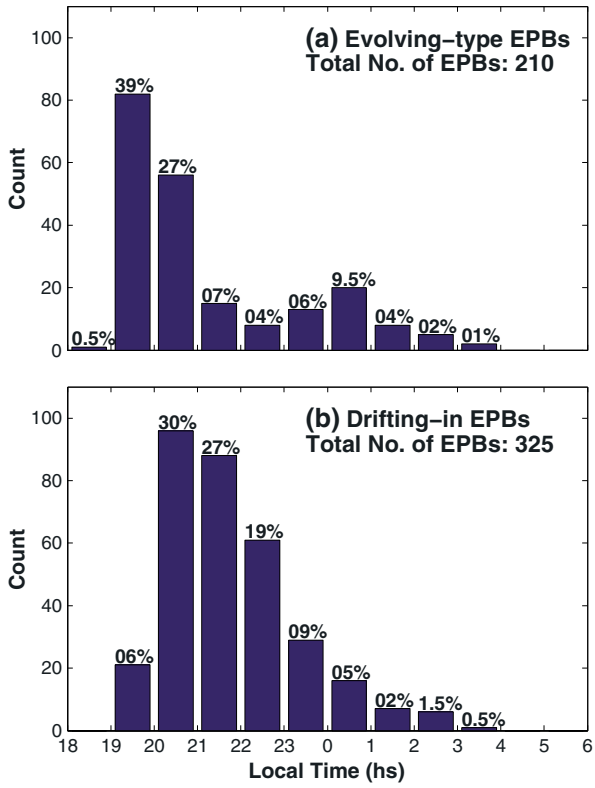

Figure 3. Histograms showing the nocturnal occurrence of (a) evolving-type EPBs and (b) drifting-in EPBs during the ascending phase of solar cycle 24 (2010–2012). The numbers shown on top of histogram bars indicate the percentage of occurrence.

An example showing the evolution of an EPB within the FoV of EAR is presented in Figure 1. It can be seen that there were no backscatter echoes at 1948 LT in Figure 1. At 1951 LT, a faint backscatter echo which is a signature of EPB can be seen around 360–400 km altitude. As time progresses, one can observe the successive growth of EPB in size and echo intensity. Further, it can also be observed that the developed EPB exhibits an eastward drift starting from 2009 LT and drifted completely out of FoV by 2100 LT. In the present study, the EPBs originated and successively grown within the FoV of EAR similar to the example shown in Figure 1 are considered as evolving-type EPBs.

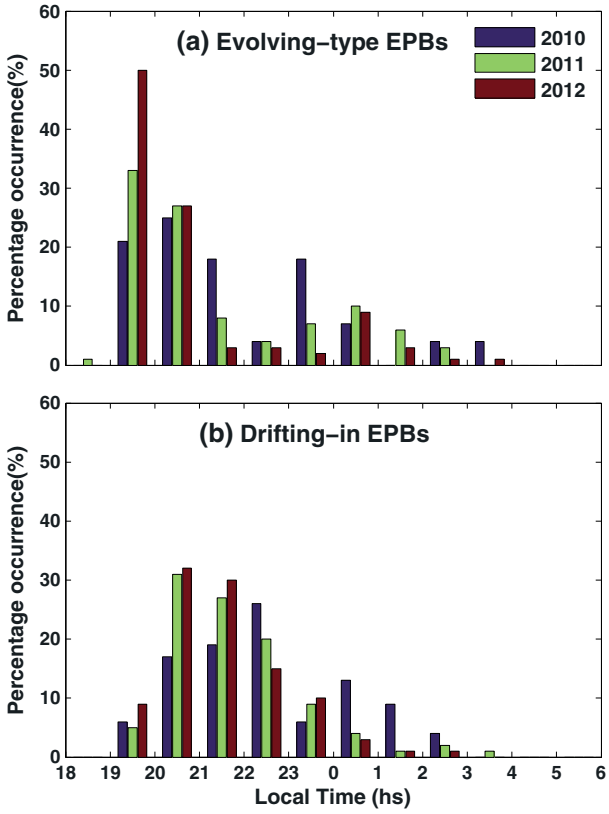

Figure 4. The nocturnal occurrence (percentage) of (a) evolving-type and (b) drifting-in EPBs during the low solar activity year 2010 and moderately higher solar activity years 2011 and 2012.

Figure 2 shows an example of drifting-in EPB where one can see a developed bubble with high echo intensity (signal-to-noise ratio) entering from western edge of FoV around 2030 LT. Subsequently, one can clearly see the bubble drifting eastward and moving out of FoV by around 2227 LT. The developed EPBs entering from either edge of FoV similar to the example shown in Figure 2 were considered as drifting-in EPB in the present study. A total of 535 EPBs were observed from EAR during 2010–2012. Each of the EPBs was individually considered and classified in to evolving-type and drifting-in bubbles as described above. The annual and seasonal occurrence statistics of both evolving-type and drifting-in EPBs are given in Table 1.

3. Results

3.1. Nocturnal Occurrence of Evolving-Type and Drifting-In EPBs

It is known that the EPBs usually develop around *F* region sunset over the magnetic equator [e.g., *Aarons et al*., 1980; *Abdu et al*., 1983; *Yokoyama et al*., 2004]. Further, it is also reported in literature that the EPBs can develop even several hours after apex sunset when there is an upwelling of equatorial *F* layer [e.g., *Tsunoda*, 2010; *Nishioka et al*., 2012]. Therefore, with a view to understand the nocturnal occurrence pattern of evolving-type and drifting-in EPBs, the EPBs observed during 2010–2012 over Kototabang were binned into 1 h intervals between 1800 and 0600 LT based on the local time of their initial appearance in FoV of radar. A total of 535 EPBs were observed by EAR during 2010–2012 out of which 210 (~39%) are of evolving-type and the remaining 325 (~61%) are of drifting-in EPBs. The histograms showing nocturnal occurrence of evolving-type and drifting-in EPBs are presented shown in Figures 3a and 3b, respectively. The numbers shown on top of histogram bars indicate the percentage of occurrence. It can be observed from Figure 3a that the evolving-type EPBs mostly occurred during 1900–2100 LT and decreases sharply to a minimum of 4% at 2200 LT. An important finding that can be noted from Figure 3a is that the evolving-type EPBs exhibit a secondary peak around midnight with 6% and 9.5% occurrences in 2300–0000 and 0000–0100 LT bins, respectively. It is also interesting to note that there were small but significant number of evolving-type EPBs observed even at late midnight hours. In case of drifting-in bubbles (Figure 3b), the number of EPBs during 1900–2000 LT bin were significantly smaller than evolving-type EPBs, and the maximum percentage of occurrence (76%) is shifted to 2000–2300 LT interval. Unlike the evolving-type EPBs, no secondary peak around midnight is observed in the occurrence of drifting-in bubbles which decreases monotonically with local time.

The annual mean $F_{10.7}$ cm solar flux increases from 80 solar flux unit (sfu) in 2010 to 116 and 120 sfu during the years 2011 and 2012, respectively. Therefore, with a view to further examine the solar activity influence, the nocturnal percentage occurrence of EPBs during the years 2010–2012 are separately presented in Figure 4. During the postsunset hours (1900–2100 LT), it can be noticed that the occurrence of both evolving-type and drifting-in EPBs (Figures 4a and 4b) is increased with increasing solar activity from 2010 to 2011–2012. However, the nocturnal occurrence pattern of evolving-type EPBs (Figure 4a) during all the years (2010–2012) show similar features with a primary peak at postsunset hours (1900–2100 LT) and a secondary peak around postmidnight hours (2300–0100 LT). In the case of drifting-in EPBs (Figure 4b), the maximum percentage of

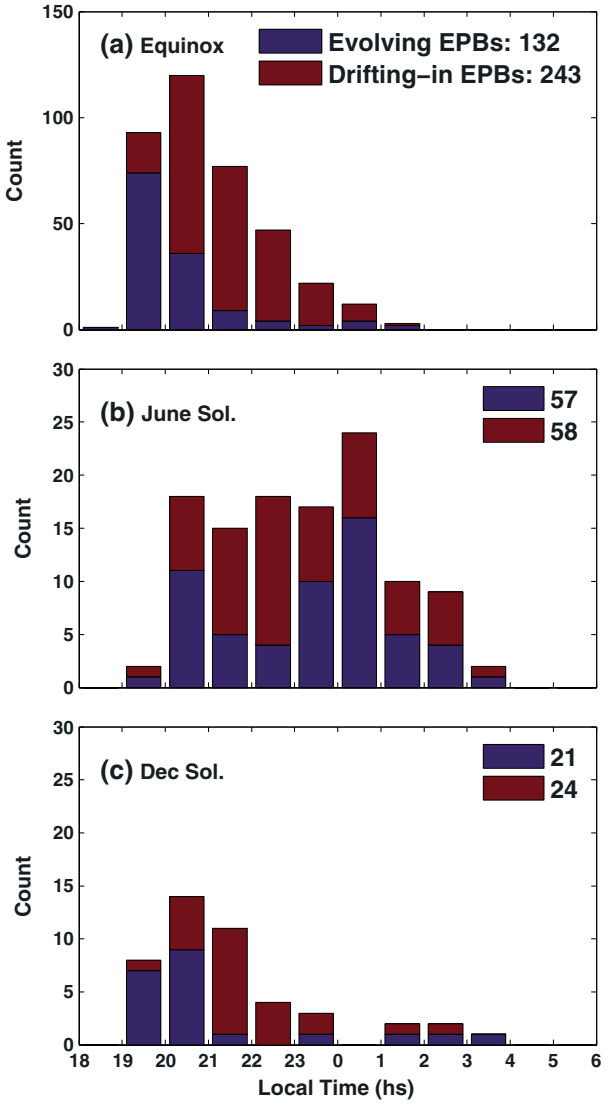

Figure 5. Seasonal variations in the nocturnal occurrence of EPBs over Kototabang during the ascending phase of solar cycle 24 (2010–2012).

occurrence is shifted to 2000–2300 LT interval for all the years. There was no clear secondary peak is observed in drifting-in EPBs during the postmidnight hours except some enhancements in the year 2010. It should be mentioned here that the number of observational days in 2010 are significantly less than in the years 2011 and 2012 (see Table 1). Therefore, considering the similar nocturnal occurrence patterns for all the three years, we combine all the EPB observations from 2010 to 2012 in the rest of our analysis.

3.2. Seasonal Occurrence of Evolving-Type and Drifting-In EPBs

In order to further examine the seasonal occurrence pattern, the EPBs observed during 2010–2012 over Kototabang were separated into equinox (March, April, September, and October), June (May–August), and December (January, February, November, and December) solstices and presented in Figure 5. During equinoxes (Figure 5a) both evolving-type and drifting-in bubbles are maximized around postsunset hours (1900–2200 LT) and decreases monotonically with local time. There was no secondary peak around midnight during equinoxes. However, during the June solstice (Figure 5b), the occurrence of evolving-type EPBs is enhanced and exhibits a clear peak around midnight. Further, the evolving-type EPBs are in fact higher than drifting-in bubbles during postmidnight. The overall occurrence of EPBs was significantly small during December solstice over Kototabang and the majority of them occur during the postsunset hours. Therefore, the results from Figures 3 and 5 indicate that a large number of EPBs observed during the postmidnight hours are freshly evolved and are primarily during June solstice.

3.3. Onset Time and Altitudes of Evolving-Type EPBs

We now focus our investigation only to evolving-type EPBs which originated and successfully grown within the FoV of EAR to further understand the probable local times and altitude regions of EPB onset during different seasons. From the fan sector backscatter maps of EAR, the longitude, altitude, and local times of EPB onset are identified. It should be mentioned here that the EPB onset referred here corresponds to the time and location (altitude and longitude) at which the ~3 m scale irregularities were seen by the EAR at their first appearance with detectable amplitude. *Basu et al.* [1978] have shown that during the generation phase of EPBs, the kilometer- and meter-scale irregularities coexist. Since the EPBs generally originate at the equator, the altitudes of the bubble onset (at first appearance) are converted to apex altitude using the field line equation. The local time of bubble onset is corrected for the longitude of EPB at their first appearance. It should be mentioned here that the EPBs observed by EAR are generally associated with topside ESF which rose to an apex altitude of ~400 km in order to

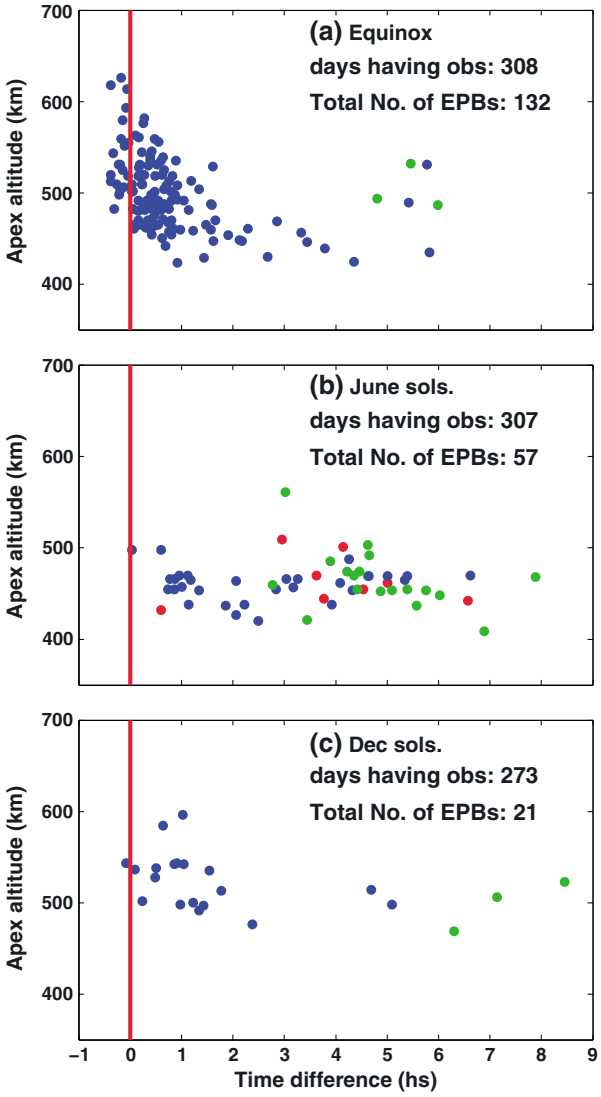

Figure 6. Apex altitudes of EPBs onset as a function of time difference between bubble onset and apex sunset. The red vertical line represents the apex sunset time. The blue dots represent the EPBs which exhibited clear eastward drift after their development. The green dots indicate EPBs which did not exhibited any clear drift, but instead decayed and slowly disappear within the FoV of radar. The red dots indicate westward drifting EPBs.

be detected at ~200 km in EAR backscatter maps. That means, the bubble whose onset takes place around *F* region altitudes will take small, but, finite time to raise up to 400 km altitude to be detected from EAR. *Dabas and Reddy* [1990] estimated that the EPB rise velocity vary ~128–416 m/s at *F* region altitudes, which indicate that the rise time is small and only ~4–13 min for an EPB initiated at apex altitude of 300 km (*F* region) to be detectable from EAR. On the other hand, the EPBs which initiated above ~400 km apex altitude would be detected immediately by the EAR.

Figure 6 shows the apex altitude of EPB onset as a function of time difference between bubble onset and apex sunset. The red vertical line represents the apex sunset time. The blue dots in Figure 6 indicate the EPBs which exhibit clear eastward drift after their development. The green dots indicate EPBs which did not exhibited any clear drift, instead, decayed and slowly disappeared within the FoV of radar. The red dots indicate westward drifting EPBs. It can be noticed from Figure 6 that there were many EPBs were found to develop even several hours after apex sunset which is in contrast to that reported by *Yokoyama et al*. [2004] and *Fukao et al*. [2006] from the EAR observations of high solar activity period.

During equinoxes (Figure 6a) the majority of the EPBs were found to evolve around the apex sunset and ~76% of EPBs are formed within 1 h from the apex sunset. It is also interesting to note that a large number of evolving-type EPBs were observed even a few minutes before the apex sunset. *Yokoyama et al*. [2004] also reported similar observations of EPBs prior to the apex sunset. The altitude of bubble onset is generally high (470–625 km) for those EPBs which developed prior to apex sunset. The onset altitude generally decreases with time after sunset with a few exceptions around midnight. Further, almost all of the bubbles observed during equinoxes exhibited eastward drift except three which slowly decayed within the FoV with no clear drift pattern. There were no bubbles observed with clear westward drift during equinoxes.

During June solstice (Figure 6b), the majority of EPBs found to develop well after apex sunset and ~86% EPBs developed after 1 h from apex sunset. The apex altitudes of EPBs onset during June solstice are generally low (~400–500 km). It can be noticed from Figure 6b that a significant number of EPBs (33%) developed during June solstice did not exhibited any clear zonal drift and about 14% EPBs exhibited westward drift. The onset times of EPBs during December solstices (Figure 6c) are mostly clustered within 2 h from the apex sunset in addition to a few that scattered during late night hours. Further, the onset altitudes of these EPBs which generated around sunset are generally high (>470 km) and they normally drift eastward. There were no EPBs

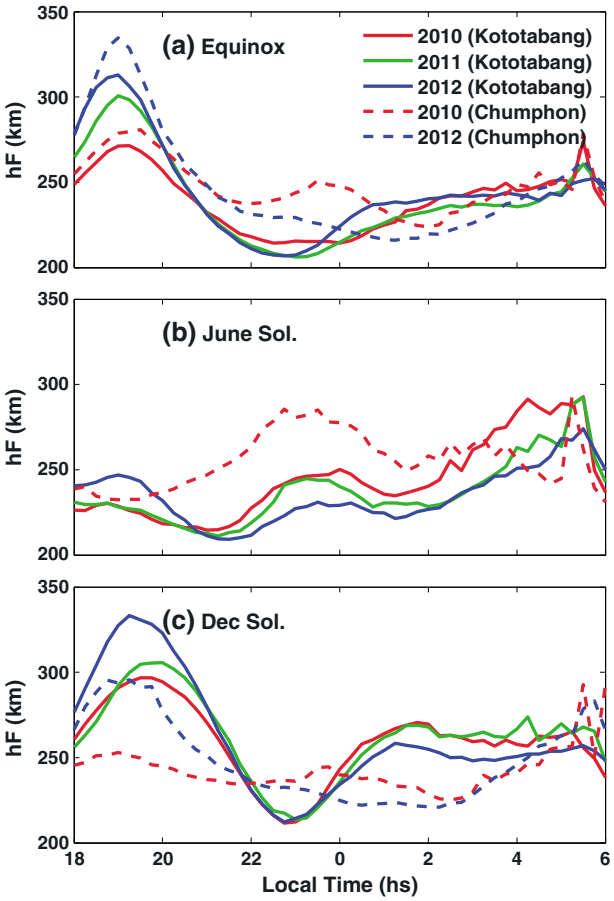

Figure 7. The nighttime mean *h'F* variation over Kototabang (solid lines) and Chumphon (dotted lines) during (a) equinox and (b) June and (c) December solstices of the years 2010–2012. The red, green, and blue curves are for the years 2010–2012, respectively.

observed with westward drift during December solstice. Therefore, the results from Figure 6 indicate that the EPBs which exhibit westward drift are confined only to June solstice.

Otsuka et al. [2009] have also reported that the postmidnight FAIs observed over Kotatabang during June solstices often tend to propagate westward (although most of them did not show clear propagation) similar to midlatitude FAIs. The nighttime eastward thermospheric wind during June solstices is very weak [*Fejer et al.*, 1991; *Liu et al.*, 2006] and may turn into westward around midnight during low solar activity periods [*Fejer*, 1993; *Biondi et al.*, 1999]. Further, *Sobral et al.* [2011] suggested that the zonal drift of irregularities may turn into westward when the thermospheric wind reverses from eastward to westward. Nevertheless, the significant number of EPBs observed during postmidnight hours June solstices did not exhibited any clear zonal drift; instead, they slowly decayed within the FoV of radar perhaps due to weak thermospheric winds during this low solar activity period. The absence of secondary peak (around midnight) in drifting-in EPBs (Figure 3b) may be due to this nondynamic character of postmidnight EPBs.

4. Discussion

The EPBs originate at equatorial latitudes through Rayleigh-Taylor (R-T) instability and rapidly evolve to topside ionosphere via polarization electric fields within them. Once developed, the EPBs generally drift eastward with ambient plasma and can cause scintillation at eastern longitudes at later local times. Hence, the explicit characteristics of EPBs at both evolutionary phase and drifting phase, and their local time and seasonal variability, are important to improve the forecasting ability of ionospheric scintillation. The rapid beam steering capability of EAR facilitates the observations of spatial and temporal evolution of EPBs over Kototabang which enabled us to classify the evolving-type EPBs and drifting-in bubbles. The results presented in Figures 3 to 6 indicate that the evolving-type EPBs during equinox and December solstice are highly populated around the postsunset hours during 2010–2012 (low to moderate solar activity period). The important observation is that a large number of EPBs observed during the postmidnight hours are freshly evolving-type and majority of them comes from June solstices. From the vector electric field instrument (VEFI) observations on board the C/NOFS, *Huang et al.* [2010] and *Yokoyama et al.* [2011b] reported that most of the postmidnight bubbles observed during 2008–2009 (low solar activity period) are associated with rapid electric field fluctuations and are of generating type. Therefore, the results presented in Figures 3 to 6 are consistent with *Huang et al.* [2010] and *Yokoyama et al.* [2011a, 2011b]. Later *Nishioka et al.* [2012] reported that the equatorial *F* layer is elevated prior to the postmidnight FAIs over Kototabang and that *F* layer uplift was not caused by eastward electric field. With a view to further understand the background *F* layer conditions, the base (virtual) height variations of *F* layer (*h'F*) from FMCW ionosondes over Kototabang and a

near equatorial station Chumphon were examined. Chumphon is located along the same meridian as Kototabang and is close to the geomagnetic equator.

Figure 7 shows the nighttime mean *h′F* variation over Kototabang (solid lines) and Chumphon (dotted lines) during equinox (Figure 7a), June (Figure 7b), and December (Figure 7c) solstices of the years 2010–2012. The Chumphon ionosonde data for the year 2011 and June solstice of 2012 were not available due to operational difficulties. It can be seen from Figure 7 that the *h′F* at both Chumphon and Kototabang exhibits pronounced postsunset rise (PSSR) due to prereversal enhancement (PRE) in the zonal electric field. Clearly, the PSSR is higher at near equatorial station Chumphon than at off-equatorial station Kotatabang and increasing with solar activity from 2010 to 2012. This explains the higher occurrence of evolving-type EPBs during the postsunset hours of equinox (Figures 3a, 4a, 5a, and 6a).

During December solstices (Figure 7c), the *h′F* over Chumphon exhibit significant PSSR during the relatively higher solar activity year 2012; however, the PSSR during the low solar activity year 2010 is very small. The significant number of EPBs observed around the postsunset hours of December solstices (Figures 5c and 6c) can be attributed to this observed PSSR over the near-equatorial station Chumphon during December solstice. Interestingly, the *h′F* increase after sunset (PSSR) at off-equatorial station Kototabang is significantly higher than at Chumphon and increases with solar activity from 2010 to 2012. This nighttime *h′F* variations over Kototabang during December solstice is similar to that reported in Figures 5c, 6a, and 9a of *Maruyama et al*. [2007] from the observations during 2004. They have explained that this uplift of *F* layer (increase of *h′F*) over Kototabang is predominantly due to transequatorial northward wind during December solstice in addition to the smaller contribution from $E \times B$ drift due to PRE. The enhancement in *h′F* after sunset increases with solar activity from 2010 to 2012 which can be attributed to increase in PRE with solar activity. Hence, the *h′F* variations shown in Figure 7 corroborate with the results of *Maruyama et al*. [2007].

From Figure 7b, it can be observed that the *h′F* over Chumphon and Kototabang does not exhibit PSSR during June solstice except a very little increase (around 1800–1900 LT) at Kototabang in 2012. The *h′F* over Kototabang generally decreases after sunset and reaches to a minimum around ~2100 LT. Later, the *h′F* increases again and exhibits broad peak between 2100 and 0130 LT with a maximum around 2300–0000 LT. The *h′F* over the near equatorial station Chumphon also exhibits similar increase starting from 2000 LT and maximizes around 2300–0000 LT. Further, the *h′F* increase at equatorial station Chumphon is much larger than at low-latitude station Kototabang. Similar increases in *h′F* around midnight at Kototabang and Chumphon during the low solar activity year 2005 were earlier reported by *Maruyama et al*. [2007]. The upwelling of *F* layer causes significant reduction in ion-neutral collision frequency (ν_{in}) and thereby increases the growth rate of R-T instability. *Subbarao and Krishna Murthy* [1994] and *Sastri* [1999] have earlier reported similar increases in *h′F* between 2000 and 0200 LT from the Indian sector which leads to enhanced growth rate of R-T instability in the postmidnight sector. *Nishioka et al*. [2012] reported that the gravity driven ($g \times B$ drift) eastward current increases with the uplift of *F* layer that contributes to the enhancement in linear growth rate of R-T instability during the postmidnight hours. Further, it can be observed from Figure 5b that the development of postmidnight EPBs is maximized around 2300–0100 LT which is consistent with the elevated *F* layer observed during June solstices (Figure 7b) at near equatorial (Chumphon) and off-equatorial (Kototabang) stations.

Several processes can contribute to the upward drift of *F* layer at both equatorial and low-latitude regions. The enhanced equatorward meridional winds during nighttime [*Harper*, 1973; *Sastri et al*., 1994] that can push the plasma along the field lines is one important contributor for the uplift of *F* layer at the off-equatorial latitudes such as at Kotatabang. The effect of equatorward wind becomes small at equatorial latitudes due to low inclination angle of field lines. However, when the meridional wind from both the hemispheres converges around magnetic equatorial region such as shown by *Maruyama et al*. [2007], it helps transporting the plasma from off-equatorial regions along the field lines to higher altitudes over the equatorial region. From Figure 7b, it can be observed that the increase in *h′F* at near equatorial station Chumphon (3.3°N geomagnetic latitude) is larger than at low-latitude station Kototabang (10.4°S geomagnetic latitude) during 2010. During the June solstice which is the northern hemispheric summer, the summer to winter transequatorial wind is much stronger that can cause larger upward transport of plasma at the northern geomagnetic latitudes. For example, *Maruyama et al*. [2008] have reported a strong equatorward (southward) wind of ~100 m/s between 2200 and 0100 LT of June solstices over Indonesian sector. Therefore, the stronger equatorward wind from the Northern Hemisphere perhaps responsible for the larger increase in *h′F* over Chumphon than at Kototabang.

The zonal electric field is generally westward during nighttime which can cause downward drift of *F* region plasma at equatorial latitudes. However, the downward drift due to westward electric field is generally weak during the postmidnight hours of June solstices, particularly, during low solar activity periods [*Fejer et al*., 1991]. One can observe from Figure 7b that the *h′F* over Kototabang between 1800 and 2100 LT is low during 2010 and increases with solar activity during 2011 and 2012. However, after ~2100 LT (the time when *h′F* starts increasing), the *h′F* is higher during 2010 and lower during 2011 and 2012 exhibiting an inverse relationship with solar activity. This is due to reversal in zonal electric field around ~2100 LT. The eastward (westward) zonal electric field during day (night) that causes the upward (downward) plasma drift generally increases with increasing solar activity [*Fejer et al*., 1991]. The increase in *h′F* from 2010 to 2012 observed during the postsunset hours in Figure 7b is mainly due to increase in eastward zonal electric field (PRE) with increasing solar activity. However, when this zonal electric field reverses to westward around ~2100 LT, the weaker westward electric fields causes smaller downward plasma drifts during the low solar activity year 2010 than during the moderately higher solar activity years 2011 and 2012. Nevertheless, the enhancement of *h′F* over Kototabang between 2100 and 0100 LT during all the three years 2010–2012 further suggests that the westward electric field is generally weak during this low to moderate level of solar activity period which cannot overcome the upward push by equatorward neutral wind. Though we do not have the data, we can expect similar increase in *h′F* over Chumphon during 2011 and 2012 as well. Another process that can possibly contribute to the apparent vertical drift of *F* layer is the recombination of bottomside plasma during nighttime. It is shown that the vertical motion of *F* layer is dominated by the recombination process, particularly, when the *F* layer heights are below 300 km [*Bittencourt and Abdu*, 1981]. Through model simulations, *Nicolls et al*. [2006] further shown that bottomside recombination will play an important role in *F* layer uplift when the westward electric field is weak. However, it can be observed from Figure 7b that after reaching a maximum around 0000 LT, the *h′F* is again showing a decrease up to 0100–0130 LT. This decrease in *h′F* is perhaps due to reduced effects of equatorward meridional winds. Later from ~0130 LT, the *h′F* is showing a continuous increase till the predawn hours which can be mainly regarded as apparent drift due to recombination at bottomside *F* layer. Therefore, the broad peak observed in *h′F* between ~2100 and 0130 LT indicates the major contribution from the equatorward wind to the uplift of *F* layer and the generation of EPBs during this period.

Another favorable factor for the generation of postmidnight EPBs is the seeding by electric field perturbations associated with medium-scale traveling ionospheric disturbances (MSTIDs) [*Otsuka et al*., 2004; *Miller et al*., 2009; *Krall et al*., 2011]. The MSTIDs generally propagate in southeast to northwest direction over Indonesian sector and maximizes during June solstices [*Otsuka et al*., 2011]. Earlier studies using EAR suggest that some of the postmidnight FAIs are midlatitude type FAIs accompanied by MSTIDs [*Yokoyama et al*., 2011a, 2011b; *Otsuka et al*., 2012]. *Yokoyama et al*. [2011b] suggested that the electric field perturbations associated with MSTIDs may play an important role in seeding of EPBs while the convergence of equatorward wind and uplift of *F* layer provide suitable conditions for the growth of R-T instability.

During equinoxes, the occurrence of evolving-type EPBs is largely concentrated around apex sunset due to postsunset rise of *F* layer associated with PRE (Figures 6a and 7a). A large number of EPBs are observed even a few minutes prior to the apex sunset (Figure 6a). The apex altitude of onset is generally high for these pre-sunset EPBs, which further indicates that the enhanced PRE is the responsible mechanism during those days. *Tulasi Ram et al*. [2014] have shown that the polarization electric fields and large-scale wave structure (LSWS) can grow a few minutes before the *F* region sunset when the field line-integrated *E* region conductivity reduces. The LSWS can greatly enhance the growth rate of R-T instability and EPBs will develop at the upwellings of the LSWS [*Tsunoda*, 2005; *Tulasi Ram et al*., 2012]. Further, *Yokoyama et al*. [2004] have shown that the 3 m scale irregularities can exist before apex sunset and are usually associated with intense bubbles that rise to high altitudes over the geomagnetic equator. Therefore, it may be possible to think that the polarization electric fields associated with the upwelling/crest of LSWS could augment the PRE and causes enhanced postsunset height rise of *F* layer [for example, *Tsunoda and Ecklund*, 2007]. This will lead to the development of EPBs even prior to the apex sunset. However, this hypothesis needs to be further validated with a detailed study. From Figure 6a, it can also be observed that there are a significant number of freshly generated EPBs after a few hours of apex sunset during equinoxes. However, from the EAR observations during high solar activity period, *Yokoyama et al*. [2004] and *Fukao et al*. [2006] have reported that the onset time of fresh EPBs is mainly confined to the period between local sunset and apex sunset during equinoxes. Therefore, while the results presented in Figure 6a corroborate with *Yokoyama et al*. [2004]

and *Fukao et al*. [2006] in terms of largely populated evolving-type EPBs around apex sunset, it differs from those in light of significant number EPBs generating even (a few hours) after the apex sunset. This difference is probably due to solar maximum conditions and limited number of observations considered in *Yokoyama et al*. [2004] and *Fukao et al*. [2006].

5. Summary

We have classified the EPBs observed over Kototabang into evolving-type and drifting-in EPBs using the rapid beam steering capability of EAR during the increasing solar activity period (2010–2012). A total of 535 EPBs were observed from the EAR over Kototabang, out of which 210 (nearly 39%) were evolved within the FoV of EAR and the other 325 (nearly 61%) were formed out of FoV and subsequently drifted in. The local time, seasonal preferences, and the zonal drift characteristics of evolving-type and drifting-in EPBs are explicitly studied, and the important findings are summarized hereunder. (i) In general, the local time occurrence of both evolving-type and drifting-in EPBs exhibits predominance around postsunset hours during this ascending phase of solar cycle. (ii) Interestingly, occurrence of evolving-type EPBs exhibits a clear secondary peak around midnight, primarily, due to higher rate of occurrence during postmidnight hours of June solstice. (iii) During postmidnight hours of June solstices, the number of evolving-type EPBs is higher than drifting-in bubbles. (iv) During equinoxes, a large number of EPBs were found to develop even a few minutes before the apex sunset and at higher apex altitudes. (v) The EPBs during equinoxes and December solstices mostly exhibited eastward drift except a few during postmidnight hours which did not exhibited any clear drift pattern. (vi) A significant number of EPBs (33%) during June solstice did not propagated, instead, slowly decayed within the FoV of radar. (vii) About 14% of EPBs during June solstice exhibited clear westward drift, and they are confined only to June solstice. These results are important for better understanding on the genesis of postmidnight EPBs and provide important insights toward improved forecasting of ionospheric scintillations.

Acknowledgments

This work is supported by Department of Science and Technology, Government of India through project GITA/DST/TWN/P-47/2013. The Equatorial Atmosphere Radar (EAR) is operated by Research Institute for Sustainable Humanosphere, Kyoto University (RISH) and Indonesian National Institute of Aeronautics and Space (LAPAN) (PI of this project M. Yamamoto may be contacted for data requests at yamamoto@rish.kyoto-u.ac.jp). This work was partly supported by JSPS KAKENHI grants 22403011, 25302007, and MEXT Strategic Funds for the Promotion of Science and Technology. The authors thank NICT, Japan for providing ionosonde data of Kototabang and Chumphon through SEALION network (PI of this project T. Yokoyama may be contacted for data requests at tyoko@nict.go.jp).

Alan Rodger thanks Eurico dePaula and another reviewer for their assistance in evaluating this paper.

References

Aarons, J., J. P. Mullen, H. E. Whitney, and E. M. Mackenzie (1980), The dynamics of equatorial irregularity patch formation, motion and decay, *J. Geophys. Res.*, *85*, 139–149, doi:10.1029/JA085iA01p00139.

Abdu, M. A., R. T. deMedeiros, J. A. Bittencourt, and I. S. Batista (1983), Vertical ionization drift velocities and range type spread F in the evening equatorial ionosphere, *J. Geophys. Res.*, *88*(A1), 399–402, doi:10.1029/JA088iA01p00399.

Basu, S., S. Basu, J. Aarons, J. P. McClure, and M. D. Cousins (1978), On the coexistence of kilometer and meter-scale irregularities in the nighttime equatorial *F* region, *J. Geophys. Res.*, *83*(A9), 4219–4226, doi:10.1029/JA083iA09p04219.

Bhattacharyya, A., S. Basu, K. M. Groves, C. E. Valladares, and R. Sheehan (2001), Dynamics of equatorial F region irregularities from spaced receiver scintillation observations, *Geophys. Res. Lett.*, *28*(1), 119–122, doi:10.1029/2000GL012288.

Biondi, M. A., S. Y. Sazykin, B. G. Fejer, J. W. Meriwether, and C. G. Fesen (1999), Equatorial and low latitude thermospheric winds: Measured quiet time variations with season and solar flux from 1980 to 1990, *J. Geophys. Res.*, *104*, 17,091–17,106, doi:10.1029/1999JA900174.

Bittencourt, J. A., and M. A. Abdu (1981), A theoretical comparison between apparent and real vertical ionization drift velocities in the equatorial F region, *J. Geophys. Res.*, *86*(A4), 2451–2454, doi:10.1029/JA086iA04p02451.

Dabas, R. S., and B. M. Reddy (1990), Equatorial plasma bubble rise velocities in the Indian sector determined from multistation scintillation observations, *Radio Sci.*, *25*(2), 125–132, doi:10.1029/RS025i002p00125.

Eccles, J. V. (1998), Modeling investigation of the evening prereversal enhancement of the zonal electric field in the equatorial ionosphere, *J. Geophys. Res.*, *103*, 26,709–26,719, doi:10.1029/98JA02656.

Fejer, B. G. (1993), F region plasma drifts over Arecibo: Solar cycle, seasonal, and magnetic activity effects, *J. Geophys. Res.*, *98*, 13,645–13,652, doi:10.1029/93JA00953.

Fejer, B. G., E. R. de Paula, S. A. Gonzalez, and R. F. Woodman (1991), Average vertical and zonal F region plasma drifts over Jicamarca, *J. Geophys. Res.*, *96*(A8), 13,901–13,906, doi:10.1029/91JA01171.

Fejer, B. G., L. Scherliess, and E. R. de Paula (1999), Effects of the vertical plasma drift velocity on the generation and evolution of equatorial Spread *F*, *J. Geophys. Res.*, *104*(A9), 19,859–19,869, doi:10.1029/1999JA900271.

Fukao, S., H. Hashiguchi, M. Yamamoto, T. Tsuda, T. Nakamura, M. K. Yamamoto, T. Sato, M. Hagio, and Y. Yabugaki (2003), Equatorial Atmosphere Radar (EAR): System description and first results, *Radio Sci.*, *38*(3), 1053, doi:10.1029/2002RS002767.

Fukao, S., T. Yokoyama, T. Tayama, M. Yamamoto, T. Maruyama, and S. Saito (2006), Eastward traverse of equatorial plasma plumes observed with the Equatorial Atmosphere Radar in Indonesia, *Ann. Geophys.*, *24*, 1411–1418.

Haerendel, G. (1973), Theory of equatorial spread F, report, Max-Planck-Inst. fur Phys. und Astrophys., Garching, Germany.

Harper, R. M. (1973), Nighttime meridional neutral winds near 350 km at low to mid-latitudes, *J. Atmos. Terr. Phys.*, *35*, 2023–2034.

Heelis, R. A., R. Stoneback, G. D. Earle, R. A. Haaser, and M. A. Abdu (2010), Medium-scale equatorial plasma irregularities observed by Coupled Ion-Neutral Dynamics Investigation sensors aboard the Communication Navigation Outage Forecast System in a prolonged solar minimum, *J. Geophys. Res.*, *115*, A10321, doi:10.1029/2010JA015596.

Huang, C. S., O. de La Beaujardiere, R. F. Pfaff, J. M. Retterer, P. A. Roddy, D. E. Hunton, Y. J. Su, S. Y. Su, and F. J. Rich (2010), Zonal drift of plasma particles inside equatorial plasma bubbles and its relation to the zonal drift of the bubble structure, *J. Geophys. Res.*, *115*, A07316, doi:10.1029/2010JA015324.

Kelley, M. C. (1989), *The Earth's Ionosphere*, *Int. Geophys. Ser.*, vol. 43, Elsevier, New York.

Krall, J., J. D. Huba, S. L. Ossakow, G. Joyce, J. J. Makela, E. S. Miller, and M. C. Kelley (2011), Modeling of equatorial plasma bubbles triggered by nonequatorial traveling ionospheric disturbances, *Geophys. Res. Lett.*, *38*, L08103, doi:10.1029/2011GL046890.

Krishna Moorthy, K., C. Ragha Reddi, and B. V. Krishna Murthy (1979), Night time ionospheric scintillations at the magnetic equator, *J. Atmos. Terr. Phys*, *41*, 123–134.

Lee, C. C., J. Y. Liu, B. W. Reinisch, W. S. Chen, and F. D. Chu (2005), The effects of the pre-reversal drift, the EIA asymmetry, and magnetic activity on the equatorial spread F during solar maximum, *Ann. Geophys.*, *23*, 745–751.

Liu, H., H. Lühr, S. Watanabe, W. Köhler, V. Henize, and P. Visser (2006), Zonal winds in the equatorial upper thermosphere: Decomposing the solar flux, geomagnetic activity, and seasonal dependencies, *J. Geophys. Res.*, *111*, A07307, doi:10.1029/2005JA011415.

Maruyama, T., M. Kawamura, S. Saito, K. Nozaki, H. Kato, N. Hemmakorn, T. Boonchuk, T. Komolmis, and C. Ha Duyen (2007), Low latitude ionosphere-thermosphere dynamics studies with ionosonde chain in Southeast Asia, *Ann. Geophys.*, *25*, 1569–1577.

Maruyama, T., S. Saito, M. Kawamura, and K. Nozaki (2008), Thermospheric meridional winds as deduced from ionosonde chain at low and equatorial latitudes and their connection with midnight temperature maximum, *J. Geophys. Res.*, *113*, A09316, doi:10.1029/2008JA013031.

Mendillo, M., J. Baumgardner, X. Pi, and P. J. Sultan (1992), Onset conditions for equatorial Spread *F*, *J. Geophys. Res.*, *97*, 13,865–13,876, doi:10.1029/92JA00647.

Miller, E. S., J. J. Makela, and M. C. Kelley (2009), Seeding of equatorial plasma depletions by polarization electric fields from middle latitudes: Experimental evidence, *Geophys. Res. Lett.*, *36*, L18105, doi:10.1029/2009GL039695.

Nicolls, M. J., M. C. Kelley, M. N. Vlasov, Y. Sahai, J. L. Chau, D. L. Hysell, P. R. Fagundes, F. Becker-Guedes, and W. L. C. Lima (2006), Observations and modeling of post-midnight uplifts near the magnetic equator, *Ann. Geophys.*, *24*, 1317–1331.

Nishioka, M., Y. Otsuka, K. Shiokawa, T. Tsugawa, Effendy, P. Supnithi, T. Nagatsuma, and K. T. Murata (2012), On post-midnight field-aligned irregularities observed with a 30.8-MHz radar at a low latitude: Comparison with F-layer altitude near the geomagnetic equator, *J. Geophys. Res.*, *117*, A08337, doi:10.1029/2012JA017692.

Otsuka, Y., K. Shiokawa, T. Ogawa, and P. Wilkinson (2004), Geomagnetic conjugate observations of medium-scale traveling ionospheric disturbances at midlatitude using all-sky airglow imagers, *Geophys. Res. Lett.*, *31*, L15803, doi:10.1029/2004GL020262.

Otsuka, Y., T. Ogawa, and Effendy (2009), VHF radar observations of night time F-region field-aligned irregularities over Kototabang, Indonesia, *Earth Planets Space*, *61*, 431–437.

Otsuka, Y., N. Kotake, K. Shiokawa, T. Ogawa, T. Tsugawa, and A. Saito (2011), Statistical study of medium-scale traveling ionospheric disturbances observed with a GPS receiver network in Japan, in *Aeronomy of the Earth's Atmosphere and Ionosphere*, *IAGA Spe. Sopron Book Ser.*, vol. 2, edited by M. A. Abdu, D. Pancheva, and A. Bhattacharyya, pp. 291–299, Springer, Dordrecht, Netherlands.

Otsuka, Y., K. Shiokawa, M. Nishioka, and Effendy (2012), VHF radar observations of post-midnight F-region field-aligned irregularities over Indonesia during solar minimum, *Indian J. Radio Space Phys.*, *41*, 199–207.

Rama Rao, P. V. S., S. Tulasi Ram, K. Niranjan, D. S. V. V. D. Prasad, S. Gopikrishna, and N. K. M. Lakshmi (2005), VHF and L-band scintillation characteristics over Indian low-latitude station, Waltair, *Ann. Geophys.*, *23*, 2457–2464.

Sastri, J. H. (1999), Post-midnight onset of spread-F at Kodaikanal during the June solstice of solar minimum, *Ann. Geophys.*, *17*, 1111–1115.

Sastri, J. H., H. N. R. Rao, V. V. Somayajulu, and H. Chandra (1994), Thermospheric meridional neutral winds associated with equatorial midnight temperature maximum (MTM), *Geophys. Res. Lett.*, *21*, 825–828, doi:10.1029/93GL03009.

Sobral, J. H. A., et al. (2011), Midnight reversal of ionospheric plasma bubble eastward velocity to westward velocity during geomagnetically quiet- time: Climatology and its model validation, *J. Atmos. Sol. Terr. Phys.*, *73*, 1520–1528.

Sridharan, R., D. Pallam Raju, and R. Raghavarao (1994), Precursor to equatorial Spread *F* in OI 630.0 nm dayglow, *Geophys. Res. Lett.*, *21*, 2797–2800, doi:10.1029/94GL02732.

Sridharan, R., S. Mala Bagiya, and S. Sunda (2012), A novel method based on GPS TEC to forecast L band scintillations over the equatorial region through a case study, *J. Atmos. Terr. Phys.*, *80*, 230–238.

Subbarao, K. S. V., and B. V. Krishna Murthy (1994), Post-sunset F region vertical velocity variations at magnetic equator, *J. Atoms. Terr. Phys.*, *56*, 59–65.

Thampi, S. V., S. Ravindran, T. K. Pant, C. V. Devasia, P. Sreelatha, R. Sridharan (2006), Deterministic prediction of post-sunset ESF based on the strength and asymmetry of EIA from ground based TEC measurements: Preliminary results, *Geophys. Res. Lett.*, *33*, L13103, doi:10.1029/2006GL026376.

Tsunoda, R. T. (1985), Control of the seasonal and longitudinal occurrence of equatorial scintillations by the longitudinal gradient in integrated *E* region Pedersen conductivity, *J. Geophys. Res.*, *90*, 447–456, doi:10.1029/JA090iA01p00447.

Tsunoda, R. T. (2005), On the enigma of day-to-day variability in equatorial Spread *F*, *Geophys. Res. Lett.*, *32*, L08103, doi:10.1029/2005GL022512.

Tsunoda, R. T. (2010), On seeding equatorial Spread *F* during solstices, *Geophys. Res. Lett.*, *37*, L05102, doi:10.1029/2010GL042576.

Tsunoda, R. T., and W. L. Ecklund (2007), On the post-sunset rise of the equatorial *F* layer and superposed upwellings and bubbles, *Geophys. Res. Lett.*, *34*, L04101, doi:10.1029/2006GL028832.

Tulasi Ram, S., P. V. S. Rama Rao, K. Niranjan, D. S. V. V. D. Prasad, R. Sridharan, C. V. Devasia, and S. Ravindhran (2006), The role of post sunset vertical drifts at the equator in predicting the onset of VHF scintillations during high and low sunspot activity years, *Ann. Geophys.*, *24*, 1609–1616.

Tulasi Ram, S., M. Yamamoto, R. T. Tsunoda, and S. V. Thampi (2012), On the application of differential phase measurements to study the zonal large scale wave structure (LSWS) in the ionospheric electron content, *Radio Sci.*, *47*, RS2001, doi:10.1029/2011RS004870.

Tulasi Ram, S., M. Yamamoto, R. T. Tsunoda, H. D. Chau, T. L. Hoang, B. Damtie, M. Wassaie, C. Y. Yatini, T. Manik, and T. Tsugawa (2014), Characteristics of large-scale wave structure observed from African and Southeast Asia longitudinal sectors, *J. Geophys. Res. Space Physics*, *119*, 1–10, doi:10.1002/2013JA019712.

Yokoyama, T., S. Fukao, and M. Yamamoto (2004), Relationship of the onset of equatorial *F* region irregularities with the sunset terminator observed with the Equatorial Atmosphere Radar, *Geophys. Res. Lett.*, *31*, L24804, doi:10.1029/2004GL021529.

Yokoyama, T., R. F. Pfaff, M. Yamamoto, Y. Otsuka, M. Nishioka, and T. Tsugawa (2011a), On postmidnight low-latitude ionospheric irregularities during solar minimum: 1. Equatorial Atmosphere Radar and GPS TEC observations in Indonesia, *J. Geophys. Res.*, *116*, A11325, doi:10.1029/2011JA016797.

Yokoyama, T., R. F. Pfaff, P. A. Roddy, M. Yamamoto, and Y. Otsuka (2011b), On post-midnight low-latitude ionospheric irregularities during solar minimum: 2. C/NOFS observations and comparison with Equatorial Atmosphere Radar, *J. Geophys. Res.*, *116*, A11326, doi:10.1029/2011JA016798.